Negative frequency tuning of a carbon nanotube nano-electromechanical resonator

P. L. Stiller, S. Kugler, D. R. Schmid, C. Strunk, and A. K. Hüttel

Institute for Experimental and Applied Physics, University of Regensburg, 93040 Regensburg, Germany

A suspended, doubly clamped single wall carbon nanotube is characterized as driven nano-electromechanical resonator at cryogenic temperatures. Electronically, the carbon nanotube displays small bandgap behaviour with Coulomb blockade oscillations in electron conduction and transparent contacts in hole conduction. We observe the driven mechanical resonance in dc-transport, including multiple higher harmonic responses. The data shows a distinct negative frequency tuning at finite applied gate voltage, enabling us to electrostatically decrease the resonance frequency to 75% of its maximum value. This is consistently explained via electrostatic softening of the mechanical mode.

INTRODUCTION

As has been shown in many both room temperature [1, 2] and low temperature measurements [3–5], suspended carbon nanotubes display excellent properties as mechanical resonator systems. Low-temperature measurements have displayed mechanical quality factors up to $Q \sim 10^5$ [3, 6] at frequencies in the megahertz to gigahertz range. Multiple higher harmonics have been observed with frequencies up to 39 GHz [7]. One additional feature of particular interest of carbon nanotube nano-electromechanical resonators is the high tunability of the resonance frequency: the particular combination of high Young's modulus [8, 9], low diameter and low mass make it possible to tune a carbon nanotube "beam resonator" all the way from the case of a hanging chain to a rope with high tensile load [2, 10] by applying electrostatic forces via gate voltages alone. As expected from the bulk beam model, the resonance frequency typically has a minimum around zero applied gate voltage, and increases at finite voltage. We report here on a particular resonator where we have observed a strong manifestation of the opposite behaviour: the resonance frequency can be tuned down to $\sim 75\%$ of its maximum value.

SAMPLE FABRICATION

Our devices are fabricated using standard lithography techniques. Base material is a highly positive doped silicon wafer with a thermally grown 550 nm silicon dioxide layer on top. Figure 1(a) displays a typical detail SEM image of the chip geometry used in our measurements. We achieve suspended and contamination-free carbon nanotubes by chemical vapor deposition growth over predefined contacts separated by etched trenches [5, 11, 12]. As contact material, we use a 40 nm thick, co-sputtered layer of a rhenium / molybdenum alloy [5, 13]. This material also serves as etch mask for the trench definition. Various geometries are used in different chip structures; in the case discussed here, the trench between the nanotube contacts was 500 nm wide and 220 nm deep. For characterization and selection, the devices are only tested electrically at room temperature. The low temperature transport experiments with suitable samples are conducted at $T_{\text{base}} = 300 \, \text{mK}$ in a helium-3 evaporation cooling system. Here, in addition to a typical Coulomb blockade measurement setup [14], a radio frequency signal for mechanical excitation is applied contact-free by an antenna nearby in the cryostat [3]. Figure 1(b) depicts a schematic of this measurement setup: we apply a bias voltage and measure the resulting current; a gate voltage is used for varying the electrochemical potential and thereby also the charge of the carbon nanotube.

BASIC ELECTRONIC CHARACTERIZATION

Figure 2(a) displays a low-temperature ($T \simeq 300 \, \text{mK}$) measurement of the current $I(V_{\text{g}})$ through our carbon nanotube sample as a function of applied gate voltage V_{g}, for constant $V_{\text{sd}} = 2 \, \text{mV}$. The sample displays the typical behaviour of a small bandgap carbon nanotube. On the hole conduction side ($V_{\text{g}} \lesssim 2.2 \, \text{V}$) we only observe few oscillations of the current and a subsequent fast transition into an open transport regime [16]. Note, however, that the overall resistance remains high ($R \simeq 180 \, \text{k}\Omega$ at $V_{\text{g}} = 0$), indicating either a high series resistance in the leads or a multi-dot structure. On the electron conduction side ($V_{\text{g}} \gtrsim 2.6 \, \text{V}$) we observe sharp Coulomb oscillations, however no clear shell structure can be observed. By additionally varying the bias voltage V_{sd} we obtain the typical "Coulomb diamond" stability diagram, see Fig. 2(b). Multiple, strongly gate-dependent inelastic cotunnelling lines without clear pattern can be observed [17, 18], hinting at a potential structure more complex than a single minimum. Also in nonlinear transport no regular shell structure can be observed. Of note in the measurement of Fig. 2(b), however, are the rounded regions marked with arrows – here, electromechanical feedback leads to self-driving of the mechanical motion in absence of an external rf driving signal [4, 5, 15].
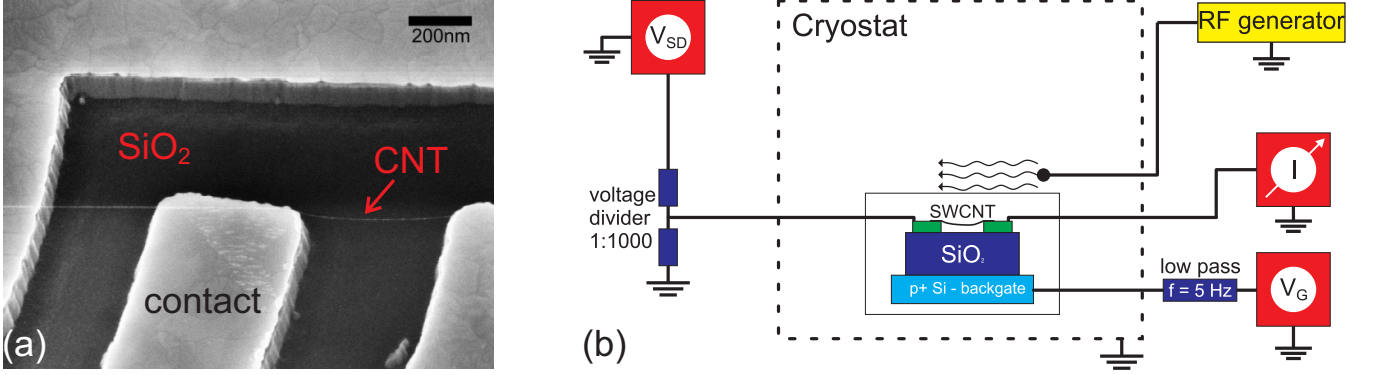
FIG. 1: (a) Detail SEM image of a typical suspended carbon nanotube sample: a suspended nanotube lies across metallized contact electrodes and the trenches etched between them. (b) Schematic of the low temperature electronic transport measurement setup; as cryostat, an Oxford Instruments helium-3 evaporation system was used.
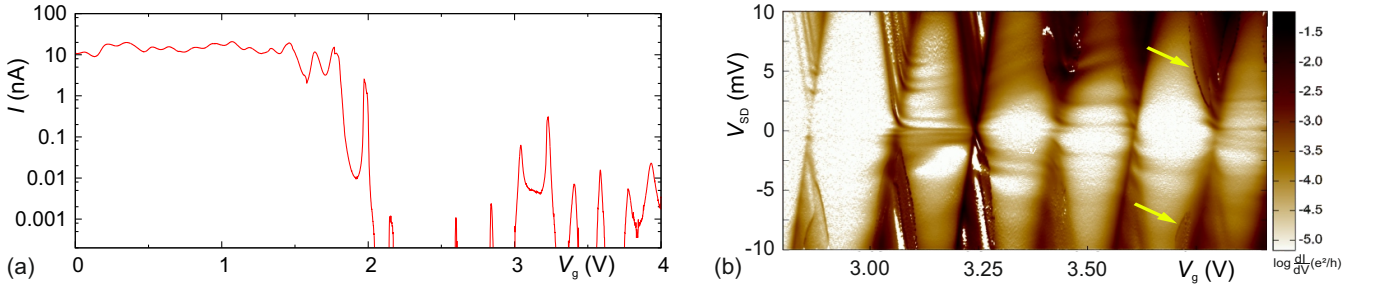

FIG. 2: (a) dc current as function of applied gate voltage V_g for constant $V_{sd} = 2\,\text{mV}$, at $T \simeq 300\,\text{mK}$. The device displays transparent behaviour in the hole regime ($V_g \lesssim 2.2\,\text{V}$), a small bandgap, and irregular Coulomb oscillations in electron conduction ($V_g \gtrsim 2.6\,\text{V}$). (b) Differential conductance dI/dV_{sd} (numerically obtained from a dc-current measurement) as function of gate voltage V_g and bias voltage V_{sd}, in the few-electron regime (logarithmical color scale). The yellow arrows mark regions of nano-electromechanical feedback [4, 5, 15].

DRIVEN MECHANICAL RESONATOR MEASUREMENTS

A mechanical resonance detection measurement is shown in Figure 3(a). The bias voltage $V_{sd} = 2\,\text{mV}$ and the gate voltage $V_g = 3.234\,\text{V}$ are kept constant, the frequency of an applied rf-signal (compare Fig. 1(b)) is varied across a large range at constant nominal generator power $P = 2\,\text{dBm}$. Since in this setup the cabling used for the radio-frequency signal is not particularly optimized, the actual power transmitted to the sample varies over the observed frequency range, leading to the large-scale oscillatory behaviour in Fig. 3(a). Mechanical resonances of the carbon nanotube show up as sharp spikes in the recorded current (for details of the detection mechanism, see e.g. [3]). We observe several resonance frequencies ranging from 72.8 MHz to 552.1 MHz. Fig. 3(b) displays an exemplary detail zoom measurement of the resonance in Fig. 3(a) around $f = 358.5\,\text{MHz}$. The width of the measured peak corresponds to a quality factor of $Q = f/\Delta f = 11800$; maximum quality factors observed on this device were $Q_{\text{max}} \simeq 72000$ at $T \simeq 300\,\text{mK}$.

Figure 3(c) shows selected extracted peak positions plotted as a function of an assigned mode number of the mechanical carbon nanotube resonator. The peaks form a sequence of approximately integer multiple frequencies; the dependence of the resonance frequency on the mode number can be fitted linearly, leading to a good agreement for $f_{\text{fit},n} = n\,(71.4 \pm 0.4)\,\text{MHz}$. This indicates the presence of a string under tension, since for the case of a hanging chain, where the bending rigidity dominates mechanical behaviour, higher vibration modes do not occur at integer multiples of the fundamental frequency [2, 10]. The observation is consistent with recent measurements on short nanotube segments [7].

In addition, in the plot of Fig. 3(a) further resonances appear. These are each marked in the plot with the resonance frequency. While a mechanical origin of these features is likely because of the sharp frequency response, a detailed identification cannot be made from our data.
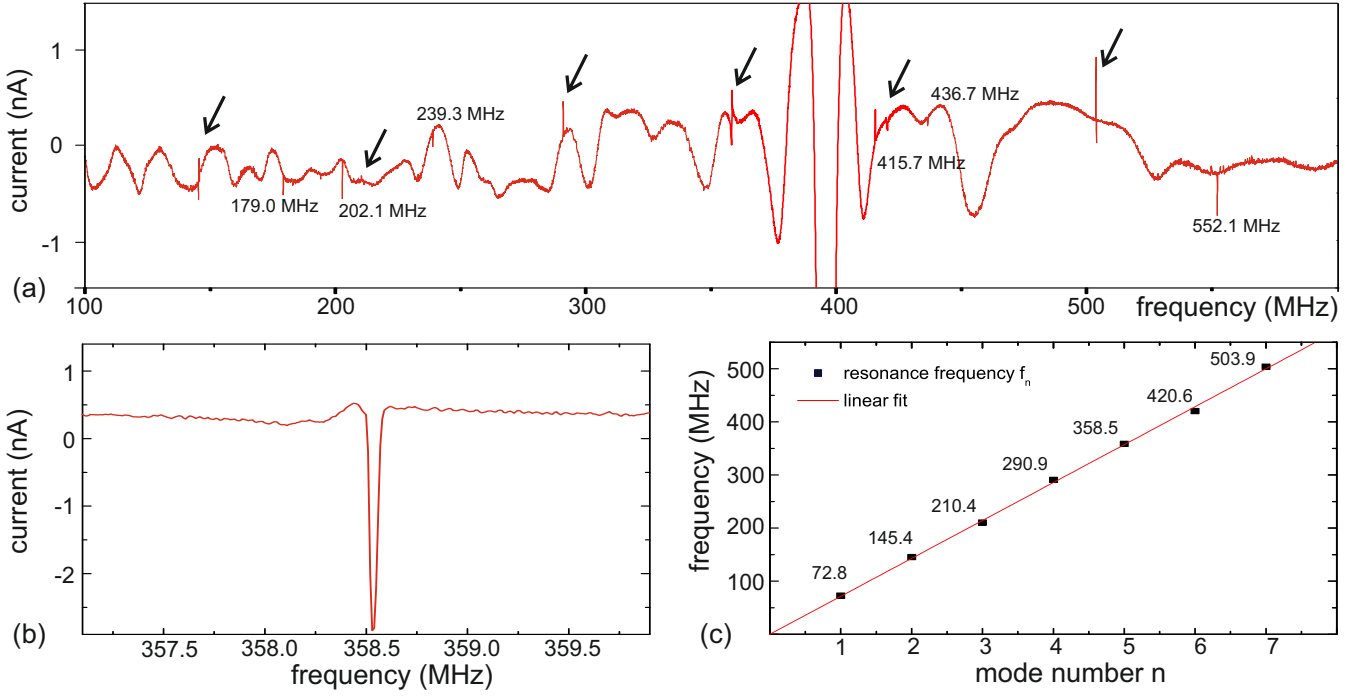
FIG. 3: (a) Time-averaged dc current through the carbon nanotube as function of the frequency of the rf driving signal, for constant $V_{\rm sd} = 2\,{\rm mV}$, $V_{\rm g} = 2.234\,{\rm V}$, and nominal rf generator power $P = 2\,{\rm dBm}$. Black arrows mark the resonance features used in the plot of (c); additionally observed resonances are marked with their frequency. (b) Detail from (a) (higher resolution measurement): exemplary resonance trace around $f = 358.5\,{\rm MHz}$. The peak width corresponds to a quality factor $Q = 11800$. (c) Selected resonance frequencies from measurements as in (a) as function of assigned mode number. A sequence of harmonics can be observed; the linear fit results in $f_{{\rm fit},n} = n\,(71.4 \pm 0.4)\,{\rm MHz}$.

GATE VOLTAGE DEPENDENCE OF MECHANICAL RESONANCE

Varying both the driving frequency f and the gate voltage $V_{\rm g}$ enables to trace the resonant features in a 2D plot. This is done in Fig. 4 for a wide gate voltage range from -12 V to 10 V. We have chosen the first harmonic frequency for this evaluation since it provides the best signal to noise ratio. As already stated, the expected behaviour would be an increase of the mechanical resonance frequency for increasing gate voltages. Fig. 4, however, displays a strong negative curvature of the resonance frequency; at $V_{\rm g} = -12\,{\rm V}$ far in the hole conduction regime the resonance frequency is reduced to approximately 75% of its maximum value. For electron conduction, the same effect emerges symmetrically.

A decrease of resonance frequency has been observed previously in literature in measurements on a suspended metallized SiC beam and on a doubly clamped InAs nanowire resonator [19, 20] and also in carbon nanotube mechanical resonators [6]. There, it is explained via so-called electrostatic softening of the vibration. For this effect, an out-of-plane motion of the carbon nanotube towards and away from the backgate is required, since the capacitance between resonator and gate electrode has to vary.

Assuming that the built-in tension in the carbon nanotube device is dominant at low gate voltage $V_{\rm g}$, we approximate that the mechanical tension and thereby the purely mechanical spring constant does not change in the observed range of $V_{\rm g}$. Following [6], we can then approximate

$$f(V_{\rm g}) = f_{\max} - \beta(V_{\rm g} - V_{g,0})^2, \qquad (1)$$

where we define with m the mass and L the length of the nanotube

$$f_{\max} = \frac{1}{2}\sqrt{\frac{T_0}{mL}}. \qquad (2)$$

The curvature of the parabola $f(V_{\rm g})$ is connected to the second derivative of the capacitance C_g between gate and resonator as function of the distance h between them, $C_g''(h) = {\rm d}^2 C_g/{\rm d}h^2$, via

$$\beta = f_{\max}\frac{C_g'' L}{4\pi^2 T_0}. \qquad (3)$$

The black dotted line in Fig. 4 corresponds to a parabolic fit using Eq. 1 with the parameters $f_{\max} = 146.9\,{\rm MHz}$, $V_{g,0} = 1.4\,{\rm V}$, and $\beta = 0.192\,{\rm MHz/V^2}$. Assuming a mass of the carbon nanotube $m = 0.17 \times 10^{-21}\,{\rm kg}$ and a nanotube length equal the trench width
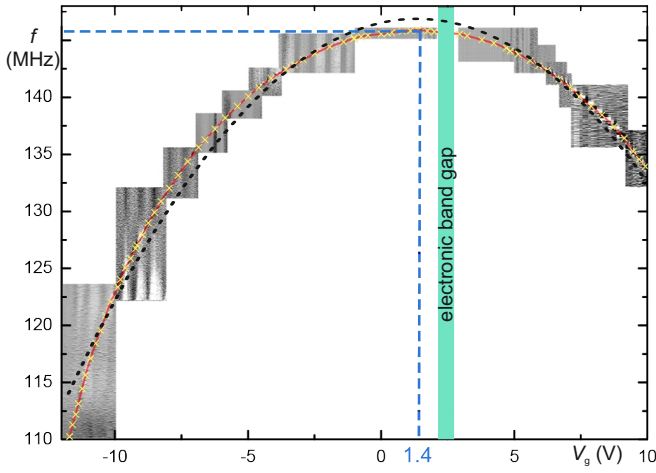
FIG. 4: Background: numerical derivative dI/df of the measured time-averaged dc current as function of external rf driving frequency f and gate voltage V_{g}, for nominal driving power $P = 0\,\mathrm{dBm}$ and bias voltage $V_{\mathrm{sd}} = 2\,\mathrm{mV}$. The extracted resonance peak positions for the first harmonic frequency f_2 as function of gate voltage V_{g} are overlaid as yellow crosses. The black dotted line corresponds to a parabolic fit, see equation 1.

$L = 500\,\mathrm{nm}$, these values lead to $T_0 = 7.3\,\mathrm{pN}$ and $C_g'' = 7.5 \times 10^{-7}\,\mathrm{F/m^2}$.

As can be seen in Fig. 4, the parabolic fit does not accurately represent the functional dependence of $f(V_{\mathrm{g}})$. Several possible mechanisms can contribute here. Eq. 1 assumes that the charge on the nanotube is proportional to the applied gate voltage, which in particular does not hold within and close to the electronic band gap. In addition the mechanical tension varies, leading to additional contributions to f.

As a consistency check, we calculate the distance between carbon nanotube and gate required to obtain this value of C_g'', using the simple model of a thin beam with radius r above an infinite conductive plane. Assuming a nanotube radius $r = 2\,\mathrm{nm}$, and L and C_g'' from above, we obtain a required distance in vacuum between nanotube and gate of $h = 1\,\mu\mathrm{m}$. In spite of the many approxmations used, this result is indeed of the correct order of magnitude, compared to a trench depth below the carbon nanotube of $220\,\mathrm{nm}$ and an additionally remaining silicon oxide layer of $380\,\mathrm{nm}$.

CONCLUSION

We measure electronic and mechanical properties of a high-quality factor carbon nanotube vibrational resonator at cryogenic temperatures. Both quantum dot behaviour and multiple driven mechanical resonances are observed. A sequence of higher harmonics occurs approximately at multiple integers of a base frequency, indicating that the nanotube resonator is under ten-

sion. The gate voltage dependence of the resonance frequency of the first harmonic $f_2(V_{\mathrm{g}})$ displays a distinct negative curvature; the frequency can be tuned from a maximum $f_2(V_g = 1.4\,\mathrm{V}) = 145.9\,\mathrm{MHz}$ down to $f_2(V_g = -11.7\,\mathrm{V}) = 110.2\,\mathrm{MHz}$. We successfully model this by electrostatic softening.

[1] V. Sazonova, Y. Yaish, H. Üstünel, D. Roundy, T. A. Arias, and P. L. McEuen, Nature **431**, 284 (2004).
[2] B. Witkamp, M. Poot, and H. van der Zant, Nano Lett. **6**, 2904 (2006).
[3] A. K. Hüttel, G. A. Steele, B. Witkamp, M. Poot, L. P. Kouwenhoven, and H. S. J. van der Zant, Nano Letters **9**, 2547 (2009).
[4] G. A. Steele, A. K. Hüttel, B. Witkamp, M. Poot, H. B. Meerwaldt, L. P. Kouwenhoven, and H. S. J. van der Zant, Science **325**, 1103 (2009).
[5] D. R. Schmid, P. L. Stiller, C. Strunk, and A. K. Hüttel, New Journal of Physics **14**, 083024 (2012).
[6] A. Eichler, J. Moser, J. Chaste, M. Zdrojek, I. Wilson-Rae, and A. Bachtold, Nature Nanotechnology **6**, 339 (2011).
[7] E. A. Laird, F. Pei, W. Tang, G. A. Steele, and L. P. Kouwenhoven, Nano Letters **12**, 193 (2012).
[8] J. P. Lu, Phys. Rev. Lett. **79**, 1297 (1997).
[9] M.-F. Yu, B. S. Files, S. Arepalli, and R. S. Ruoff, Phys. Rev. Lett. **84**, 5552 (2000).
[10] A. N. Cleland, *Foundations of Nanomechanics* (Springer Verlag, 2003).
[11] J. Cao, Q. Wang, and H. Dai, Nature Materials **4**, 745 (2005).
[12] G. A. Steele, G. Götz, and L. P. Kouwenhoven, Nature Nanotechnology **4**, 363 (2009).
[13] B. H. Schneider, S. Etak, H. S. J. van der Zant, and G. A. Steele, Scientific Reports **2**, 599 (2012).
[14] L. P. Kouwenhoven, C. M. Marcus, P. L. McEuen, S. Tarucha, R. M. Westervelt, and N. S. Wingreen, *Electron transport in quantum dots* (Kluwer, 1997).
[15] O. Usmani, Y. M. Blanter, and Y. V. Nazarov, Phys. Rev. B **75**, 195312 (2007).
[16] W. Liang, M. Bockrath, D. Bozovic, J. H. Hafner, M. Tinkham, and H. Park, Nature **411**, 665 (2001).
[17] S. De Franceschi, S. Sasaki, J. M. Elzerman, W. G. van der Wiel, S. Tarucha, and L. P. Kouwenhoven, Phys. Rev. Lett. **86**, 878 (2001).
[18] K. Goß, S. Smerat, M. Leijnse, M. R. Wegewijs, C. M. Schneider, and C. Meyer, Phys. Rev. B **83**, 201403 (2011).
[19] I. Kozinsky, H. W. C. Postma, I. Bargatin, and M. L. Roukes, Applied Physics Letters **88**, 253101 (pages 3) (2006).
[20] H. S. Solanki, S. Sengupta, S. Dhara, V. Singh, S. Patil, R. Dhall, J. Parpia, A. Bhattacharya, and M. M. Deshmukh, Phys. Rev. B **81**, 115459 (2010).